JGR Oceans

RESEARCH ARTICLE

10.1029/2024JC021655

Observations of Estuarine Salt Intrusion Dynamics During a Prolonged Drought Event in the Rhine-Meuse Delta

Tess M. Wegman[1], Julie D. Pietrzak[1], Alexander R. Horner-Devine[2], Henk A. Dijkstra[3], and David K. Ralston[4]

[1]Department of Hydraulic Engineering, Delft University of Technology, Delft, The Netherlands, [2]Department of Civil and Environmental Engineering, University of Washington, Seattle, WA, USA, [3]Department of Physics, Institute for Marine and Atmospheric Research Utrecht, Utrecht University, Utrecht, The Netherlands, [4]Woods Hole Oceanographic Institution, Falmouth, MA, USA

Key Points:

- On a weekly timescale, the river discharge is the best predictor for salt intrusion length
- Variations of salt intrusion length on a timescale of a few days are driven by coastal set-up
- Treating distributary side branches separately is crucial to incorporate the importance of downstream salinity variability

Supporting Information:

Supporting Information may be found in the online version of this article.

Correspondence to:

T. M. Wegman,
t.m.wegman@tudelft.nl

Citation:

Wegman, T. M., Pietrzak, J. D., Horner-Devine, A. R., Dijkstra, H. A., & Ralston, D. K. (2024). Observations of estuarine salt intrusion dynamics during a prolonged drought event in the Rhine-Meuse Delta. *Journal of Geophysical Research: Oceans*, *129*, e2024JC021655. https://doi.org/10.1029/2024JC021655

Received 1 AUG 2024
Accepted 4 DEC 2024

Author Contributions:

Conceptualization: Tess M. Wegman, Julie D. Pietrzak, Alexander R. Horner-Devine, David K. Ralston
Data curation: Tess M. Wegman
Formal analysis: Tess M. Wegman
Funding acquisition: Julie D. Pietrzak
Investigation: Tess M. Wegman, Alexander R. Horner-Devine, David K. Ralston
Methodology: Tess M. Wegman
Resources: Julie D. Pietrzak, Alexander R. Horner-Devine, David K. Ralston
Software: Tess M. Wegman
Supervision: Julie D. Pietrzak, Alexander R. Horner-Devine, Henk A. Dijkstra
Visualization: Tess M. Wegman
Writing – original draft: Tess M. Wegman

Abstract Salt intrusion poses a global threat to estuaries and deltas, exacerbated by climate change, drought, and sea level rise. This observational study investigates the impact of river discharge, wind, and tidal variations on salt intrusion in a branching river delta during drought. The complexity and spatial extent of deltas make comprehensive measurements challenging and rare. In this paper, we present a 17-week data set of a historic drought in the Rhine-Meuse Delta, capturing dynamics in a multiple-channel system in a wide range of conditions. Key characteristics of this low-lying delta are its branching channel network and complicated, human-controlled discharge. Despite the system's complexity, we found that the subtidal salt intrusion length, defined by the 2 PSU isohaline (L_2), follows a power law relationship with Rhine River discharge ($L_2 \propto Q_R^{-0.35 \pm 0.03}$). Subtidal water level variations contribute to short-term variations in intrusion length, shifting the limit of salt intrusion upstream and downstream with a distance similar to the tidal excursion length. This can be attributed to the up-estuary transport of seawater, caused by the estuary adjusting to variations in water levels at its mouth. However, spring-neap variation in the tidal range does not alter the subtidal salt intrusion length. Side branches exhibit distinct dynamics from the main river, and their most important control is the downstream salinity. We show that treating the side branches separately is crucial to incorporate the highly variable downstream boundary condition, and may apply in other deltas or complex estuaries.

Plain Language Summary An estuary is where saline seawater and fresh river water mix. During low river flow, seawater can be transported far upriver, known as salt intrusion, which is exacerbated by climate change. To quantify salt intrusion, we examine the distance seawater travels upriver: the salt intrusion length. This observational study explores how salt intrusion length is affected by river discharge, winds, and tides in the Rhine-Meuse Delta, the Netherlands. This estuary is more complex than most single-channel estuaries, because of its branching channel network and human-controlled discharge. We show that the salt intrusion length mainly depends on the Rhine River discharge. Water level variations associated with storm surges contribute to short-term variations in salt intrusion length. However, the tidal variations, caused by the spring-neap cycle do not alter the tidally averaged salt intrusion length. Side branches behave differently from the main river, and their salt intrusion length mainly depends on the downstream salinity. We show that treating the side branches separately is crucial to take this into account. Our findings highlight the importance of understanding how forcing conditions influence salt intrusion in a complex, branched delta, especially under drought conditions, which are likely to happen more often due to climate change.

1. Introduction

Estuaries connect saline seawaters and fresh river waters, creating unique coastal systems. Estuaries are vital for many people globally, as they usually house many inhabitants and industrial activities. When saline seawater is advected far inland, it intrudes into what are normally freshwater regions. This can cause major problems, increasing the stress on the freshwater supply for industry, agriculture, and drinking water. The extent to which saline waters enter the estuary, referred to as the salt intrusion length, is influenced by the estuary's geometry and forcing conditions. Due to variations in forcings such as river discharge, tides, winds, and mean sea level, the salt intrusion length can vary significantly within the estuary (MacCready & Geyer, 2010).

Due to a changing climate, delta regions may experience an intensification of salt intrusion, attributed to rising mean sea levels, a decrease in low flow river discharge (Kay et al., 2018; J. Lee et al., 2024), or a combination of

Writing – review & editing: Julie D. Pietrzak, Alexander R. Horner-Devine, Henk A. Dijkstra, David K. Ralston

both. In future discharge projections, the occurrence of extreme salt intrusion events in many European estuaries is expected to increase by a factor of five by the end of the 21st century (J. Lee et al., 2024). Similar trends are anticipated globally, for example, in the Mekong Delta (Eslami et al., 2019; Eslami, Hoekstra, Minderhoud, et al., 2021), the Yangtze Estuary (Dai et al., 2011), the Bengal Delta (Sherin et al., 2020), and the Pearl River Estuary (Hong et al., 2020; Liu et al., 2019). Besides the effects of climate change, direct anthropogenic drivers leading to sediment starvation, and deeper channels, can exacerbate salt intrusion (Eslami et al., 2019; Eslami, Hoekstra, Kernkamp, et al., 2021).

The salinity distribution in an estuary can be described by the balance between salt export by advection due to river discharge, and salt import by the baroclinically driven exchange flow and dispersion processes by the tides (e.g., Chatwin (1976); Hansen and Rattray (1965); MacCready (2004)). To evaluate the impact of forcing conditions such as river discharge, winds, and the spring-neap tidal cycle on salt intrusion, it is useful to examine the subtidal response of an estuary because they act on timescales longer than a single tidal cycle (Jay, 2010).

The estuarine response time varies seasonally with discharge and has been examined by, for example, Chawla et al. (2008), Cook et al. (2023), McKeon et al. (2021), Monismith et al. (2002), and Ralston et al. (2010). Salt intrusion length depends strongly on the amount of discharge, where this relationship becomes stronger as discharge increases (Abood, 1974; Cook et al., 2023; Ralston et al., 2010). The sensitivity of the salt intrusion to spring-neap variation in tides can exhibit seasonal differences because it depends, among other factors, on the response time of the estuary. The response time depends on the river flow and length of the estuary (Lerczak et al., 2009; MacCready, 2007), so during droughts the response time may be long compared to the spring-neap cycle. For example, the salt intrusion length in the Hudson River Estuary becomes insensitive to the spring-neap cycle during droughts, because the response time is 10 times larger than during moderate flow and thus much longer than the spring-neap cycle (Bowen & Geyer, 2003; Lerczak et al., 2009).

Besides the discharge and tides, winds can also influence the salt intrusion length. Winds can induce subtidal water level fluctuations, influencing the barotropic pressure gradient between the ocean and the estuary. Large up-estuary volume fluxes can be generated due to these variations in the subtidal water level. These can be in the order of magnitude of the river runoff (de Nijs et al., 2008; Ralston et al., 2008; Wong & Valle-Levinson, 2002), and thereby affect salinity concentrations throughout the estuary (Cook et al., 2023; de Nijs et al., 2008; Eslami, Hoekstra, Kernkamp, et al., 2021; Li & Li, 2011; Manca et al., 2014; Perales-Valdivia et al., 2018; Zhu et al., 2020).

The focus area of this study is the Dutch Rhine-Meuse Delta, a large, urbanized river delta with a branching channel network. Compared to single-channel estuaries, these systems include a more complex discharge distribution, different channel geometries, abrupt depth changes, and more complex tidal phase differences (Alebregtse & de Swart, 2016; Cox et al., 2021; Hill & Souza, 2006). This could introduce additional processes relevant to salt intrusion dynamics. For instance, the mixing of water masses in side channels, which is similar to tidal trapping and may lead to tidal dispersion, as described by for example, Stacey et al. (2001) and MacVean and Stacey (2011). This can be a dominant term in multichannel estuaries, as shown for the Coos Estuary by Conroy et al. (2020), and it can be further enhanced by exchange flow between side channels and the main channel (Garcia et al., 2022). Additionally, reversals in along-channel salinity gradients can occur at channel junctions (Conroy et al., 2020), which can lead to subtidal along-channel flow convergence (for example, MacVean and Stacey (2011), Warner et al. (2002). Furthermore, different responses to forcing for different branches could arise. Eslami, Hoekstra, Kernkamp, et al. (2021) showed for the Mekong Delta that the stratified branches have a clear spring-neap variability in stratification and salt flux, while some well-mixed channels do not exhibit this response.

High-resolution numerical models provide valuable insights into detailed estuarine dynamics, but only if they are well validated. Field observations are essential for validating these models and understanding the key dynamics of estuarine systems. In deltaic systems or multichannel systems, it is particularly challenging to obtain a data set that captures the spatial and temporal extent required to obtain a deep understanding of the salt intrusion dynamics. Analytical approaches aim to simplify systems to a core set of dynamics, making it easier to study the responses to forcing variability and comparisons among different systems. Analytic modeling studies of salt wedge dynamics date back more than half a century (e.g., Schijf and Schönfeld (1953)) and remain an active area of research (e.g., Poggioli and Horner-Devine (2015)). However, observations that capture the spatial and temporal variability of salt wedge dynamics are rare, especially during the extreme conditions when they are most impactful.

The Rhine-Meuse Delta estuary is the only permanently open connection between the Rhine and Meuse rivers and the North Sea, characterized as a salt wedge estuary (de Nijs et al., 2011). The Rhine-Meuse Delta is densely populated and intensively used for agriculture and industry. The most downstream section of the estuary, the Rotterdam Waterway, is the approach channel to Europe's largest harbor (Port of Rotterdam), and undergoes regular dredging for shipping. It is extensively managed by the government and regional water boards, to ensure an adequate freshwater distribution for all stakeholders.

Here, we examine salt intrusion length variations in this heavily engineered delta, focusing on extremely low river discharge conditions. We analyze a data set from the Rhine-Meuse Delta estuary collected during the severe drought of 2022, featuring the lowest ever recorded Rhine discharge. We investigate the dominant forcing mechanisms driving salt intrusion in a salt wedge estuary experiencing drought, and examine how this differs in two upstream side branches.

In Section 2, we first describe the theory of the subtidal salt balance. In Section 3, we describe the observational measurement campaign. In Section 4, we explain how the subtidal salt intrusion length depends on the observed river discharge, winds, and tides. In Sections 5 and 6, we discuss the results and present the conclusions.

2. Subtidal Salt Balance Theory

The subtidal salt balance discussed in this section assumes small salinity variations with depth, which applies to partially mixed and well-mixed estuaries. However, the Rhine-Meuse Delta is a salt wedge estuary, but the upstream branches are partially-mixed to well-mixed, which makes this approach applicable to this study. Other salt wedge estuaries have also experienced well-mixed regions during low discharge (e.g., Merrimack River Estuary in Ralston et al. (2010)).

A solution for salt intrusion length can be found in the balance for a partially mixed estuary by considering the depth-averaged and tidally averaged, salt conservation balance (Hansen & Rattray, 1965; MacCready, 2004). We can express this as a volume-integrated salt budget when the balance is integrated between the estuary mouth ($x = 0$) and the salt intrusion limit ($x = L_s$) (MacCready, 2004):

$$\underbrace{\frac{1}{A}\frac{d}{dt}\int_0^{L_s} A\bar{s}dx}_{s_1} = -\underbrace{\bar{u}\bar{s}}_{s_2} - \underbrace{\overline{u's'}}_{s_3} + \underbrace{K_h\frac{\partial \bar{s}}{\partial x}}_{s_4}, \quad (1)$$

Here, the velocity u and salinity s distribution are split into a depth-averaged and a depth-varying component, $u = \bar{u}(x) + u'(x,z)$ and $s = \bar{s}(x) + s'(x,z)$, A is the cross-sectional area of the estuary, and K_h is the along-channel diffusion coefficient. The term s_1 represents the speed of the salt intrusion length $\frac{dL_s}{dt}$, and is balanced by s_2, s_3, and s_4. Here s_2 is advection by river flow, s_3 is transport by exchange flow, and s_4 is salt import by tidal dispersion.

In terms of understanding salt intrusion length, we also examine how the speed of the intrusion is affected by different mechanisms. This intrusion speed is relevant on shorter timescales (e.g., a few days). A steady-state solution for the salt intrusion length L_s can be found for $s_1 = 0$. This holds for a timescale long enough to average over the shorter-term fluctuations.

A steady-state solution for the salt intrusion length L_s as a function of river discharge Q_R can be found in the form $L_s \propto Q_R^{-n}$. Estuaries dominated by exchange flow have an exponent of $n = \frac{1}{3}$, which assumes a dependency of K_h on the along-channel salinity gradient (Hansen & Rattray, 1965; MacCready, 1999; Monismith et al., 2002). For estuaries dominated by tidal dispersion, it is assumed that there is no K_h dependency on the along-channel salinity gradient, resulting in an exponent of $n = 1$ (Monismith et al., 2002). Salt wedge estuaries have values around $n = 2$, based on the arrested salt wedge theory (Geyer & Ralston, 2012; Schijf & Schönfeld, 1953).

The dependence of salt intrusion length on the tidal range and winds can be illustrated by the salt fluxes described in Equation 1. The spring-neap response of an estuary depends on the dominant salt flux mechanisms. Stronger tides weaken the exchange flow and stratification and thus reduce the steady salt flux (e.g., Geyer et al. (2020); Ralston et al. (2008)), and vice versa. Increasing tidal range also causes greater tidal dispersion, thereby the landward salt flux could be increased (Ralston et al., 2010). In many estuaries, along-estuary wind can either

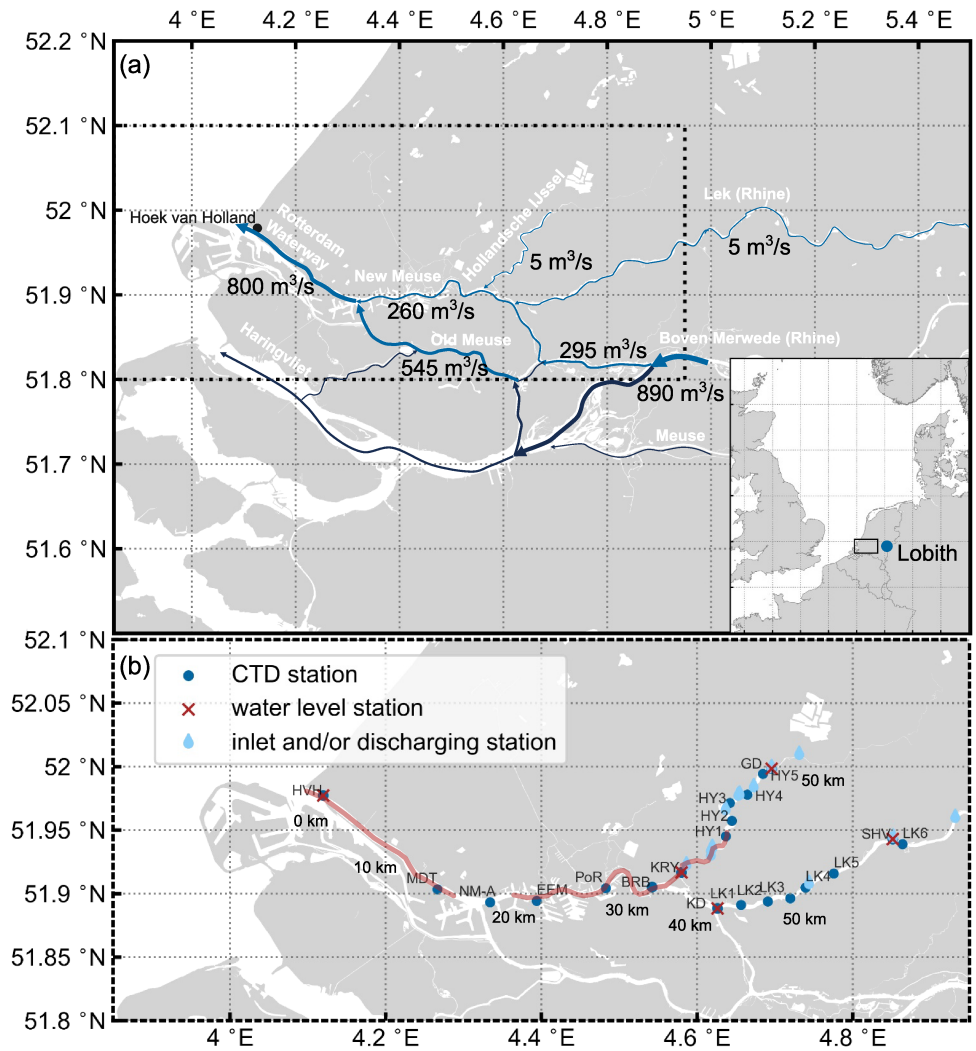

Figure 1. (a) Overview of the Rhine-Meuse Delta, and its location within Europe. For the relevant branches, the names and approximate discharges are indicated. The arrows scale with the discharges (m^3/s) based on a low Rhine River discharge scenario ($Q_R < 1000$ m^3/s at Lobith) of Cox et al. (2021). (b) An overview of the measurement locations, where conductivity, temperature, and depth (CTD) sensors in the estuary are indicated with dots (•). Stations of Rijkswaterstaat (Dutch Ministry of Infrastructure and Water Management) are sensors fixed to a reference: Hoek van Holland (HVH), Brienenoordbrug (BRB), Krimpen aan den IJssel (KRY), and Kinderdijk (KD). In the Lek (LK), six sensors were deployed 1 m below the water surface, and in the Hollandsche IJssel (HY), five sensors were deployed 1 m above the river bed. Red crosses (×) indicate water level stations. The red lines indicate the two ship transects.

enhance or reduce the exchange flow (Geyer, 1997; Hansen & Rattray, 1965; Scully et al., 2005), where down-estuary wind enhances the estuarine circulation, promoting up-estuary salt transport, and vice versa.

3. Observations

3.1. The Rhine-Meuse Delta

The Rhine-Meuse Delta Estuary is a macrotidal salt wedge estuary (de Nijs et al., 2011), located in the Netherlands. The Rhine River enters the Netherlands at Lobith (see Figure 1a), and it enters the domain of the

field measurements in the branches which are named Lek and Boven Merwede. The Meuse enters the Netherlands in the southeast, and is also indicated in Figure 1a.

The main branch of the system is the Rotterdam Waterway, which discharges into the North Sea. The most downstream junction branches into the Old Meuse (south) and the New Meuse (north). The New Meuse carries roughly 1/3 of the total Rotterdam Waterway discharge for a low discharge scenario (Cox et al., 2021), see Figure 1a. The New Meuse has branches to the Hollandsche IJssel at 36 km upstream of the mouth and to the Lek at 41 km of the mouth. These side branches, which both have low discharge from upstream during low discharge scenarios, are particularly vulnerable to salt intrusion. Figure 1a gives an overview of the estimated discharges for a low discharge scenario of the most important branches, based on 1D numerical simulations (Cox et al., 2021).

The entire Dutch river system is regularly dredged to maintain the navigation depth. The stretch of roughly 25 km of the waterway has a navigation depth of about −17 m NAP (Normaal Amsterdams Peil). Upstream of the major harbor basins, the river is shallower and the depths decrease from −14 m NAP to −5 m NAP. The Hollandsche IJssel is a dammed-off river branch with a length of 20 km, an average water depth from −4 to −4.5 m NAP, and a channel width of 50–100 m (Rijkswaterstaat, 2024a). The Lek is part of the Rhine River and has a weir (Hagestein) at 42 km from its mouth (not shown in Figure 1). The average water depth and channel width of the Lek are −5.3 m NAP and 180–330 m, respectively (Rijkswaterstaat, 2024b). Water level and salinity data are monitored at the mouths of both branches, Krimpen a/d IJssel and Kinderdijk (KRY and KD, indicated by red crosses in Figure 1b). The total discharge through the branches depends on the upstream inputs (Hagestein for the Lek, Gouda (GD) for Hollandsche IJssel) and several water extraction locations along the branches (blue droplets in Figure 1b). Hereafter, the total discharge through those branches is therefore referred to as controlled discharge.

3.2. Instrumentation

We measure the salinity based on conductivity, temperature, and depth (CTD) sensors monitoring at 20 locations in the Rhine-Meuse Delta estuary from 22 June to 19 October 2022. Most of these monitoring stations are permanent or seasonal stations of Rijkswaterstaat (Dutch Ministry of Infrastructure and Water Management), and three stations were installed for the purpose of this study.

We installed CTD sensors at the top and the bottom of the water column at four locations within the estuary. The sensors were attached to a fixed point on a quay wall at the Port of Rotterdam (PoR), and to a buoy at NM-A, and Eemhaven (EEM). Temporary sensors were also installed on a floating platform during the Maasdeltatunnel (MDT) construction by the BAAK consortium. Rijkswaterstaat deployed a salinity monitoring net in two rivers branching off the main channel: the Hollandsche IJssel (HY) and the Lek (LK). In the Lek, six sensors were installed 1 m below the water surface, and in the Hollandsche IJssel, five sensors were placed 1 m above the river bed. These depths were chosen because the water column is usually well mixed in those branches, which was confirmed in our observations (e.g., Figure 3b). The remaining salinity data were retrieved from permanent measurement stations of Rijkswaterstaat, including Hoek van Holland (HVH), Brienenoordbrug (BRB), Krimpen a/d IJssel (KIJ), and Kinderdijk (KD). The BRB station also has a 45-year time series, which is used to evaluate the drought of 2022 in terms of the historical record. All sensors and their locations are summarized in Table 1. Furthermore, two ship surveys were conducted to gain insight into the along-channel salinity structure. During those surveys, we took vertical CTD casts in the thalweg every 1,000 m. The first survey was on the 1st of August in the Rotterdam Waterway. The second survey was partially in the New Meuse and the Hollandsche IJssel on the 4th of August.

The Rhine River discharge data at Lobith (Dutch reference location, see Figure 1a) were retrieved from the Rijkswaterstaat database, as well as the water level and astronomical tide at HVH. To obtain the set-up at HVH, the water level is filtered with a low-pass Godin filter (Godin, 1972). This filter is obtained by subsequently taking the convolution of two running means of 24 hr, and the convolution of this triangular filter with a running mean length of 25 hr. Data on wind speed, wind direction, and atmospheric pressure at HVH were retrieved from the Royal Netherlands Meteorological Institute (KNMI). The controlled discharges in the branches are a combination of discharge records of Rijkswaterstaat and water boards.

To define the drought, we set a percentile threshold of 10% of the climatological discharge to identify a 'severe drought', based on NOAA's National Weather Service and methods (Hammond et al., 2022). We took a variable

Table 1
Overview of Measurement Stations Within the Estuary

Station	Distance from mouth [km]	Branch	Parameter
HVH	0	main	salinity (3 depths)
			water level
MDT	13.2	main	salinity (2 depths)
EEM	22.2	main	salinity (2 depths)
NM-A	18	main	salinity (2 depths)
PoR	28.5	main	salinity (2 depths)
BRB	35	main	salinity (2 depths)
KRY	37	Hollandsche IJssel	salinity (2 depths)
			water level
HY1	44	Hollandsche IJssel	salinity (1 depth)
HY2	45.5	Hollandsche IJssel	salinity (1 depth)
HY3	48	Hollandsche IJssel	salinity (1 depth)
HY4	49.7	Hollandsche IJssel	salinity (1 depth)
HY5	52	Hollandsche IJssel	salinity (1 depth)
GD	52.5	Hollandsche IJssel	water level
			discharge
KD	41.2	Lek	salinity (1 depth)
			water level
LK1	43.3	Lek	salinity (1 depth)
LK2	45.8	Lek	salinity (1 depth)
LK3	47.8	Lek	salinity (1 depth)
LK5	52.2	Lek	salinity (1 depth)
LK6	79.5	Lek	salinity (1 depth)
SHV	78.5	Lek	water level
Hagestein	83	Lek	water level
			discharge

drought metric, the percentile threshold for every day of the year, based on a climatological baseline period of the years 1992–2021. We compare a 5-day means of the 2022 data against these thresholds.

3.3. Estimation of the Salt Intrusion Length

To estimate the salt intrusion length (L_2), defined here as the location of the 2 PSU isohaline, we use the near-bottom salinity sensors from the estuary. The salinity between the two sensors, where the threshold value of 2 PSU is identified, is linearly interpolated to determine the salt intrusion length. The main channel (Rotterdam Waterway and New Meuse) branches off into the Hollandsche IJssel and the Lek, so a salinity intrusion length can be defined for each branch. For simplicity, the salt intrusion length in the Lek (L_2) will be used in the main analysis. In the analysis of the side branches, we chose the 0.3 PSU isohaline, because the 2 PSU isohaline does not reach the branches often. These two different intrusion limits are defined to make a distinction between the side branches and the main system. In this study, we only consider the Rhine discharge and not the Meuse discharge, because the contribution of the Meuse waters, which discharge into the North Sea through the Rotterdam Waterway is small compared to the Rhine River discharge. Lobith is chosen as a discharge reference because it represents the total Dutch Rhine discharge and an important reference location with a long-term record. To evaluate the effect of forcing conditions on the salt intrusion length, first, the time series at a frequency of 10 min is shifted in time to obtain the highest correlation between the compared quantities. This step is taken to account for the travel time of the forcing into the estuary and a lag between the forcing and the salt intrusion

response. Most lags were between 5 and 11 hr, and 10 days for the lag between salinity at BRB and salt intrusion length in the HY. Hereafter, all time series are tidally averaged, to obtain one data point per tidal cycle.

4. Results

4.1. Forcing Conditions

The forcing conditions during the study period are shown in Figure 2. The Rhine River discharge at Lobith Q_R varied between approximately 670 and 2,100 m^3/s during the measurement period (Figure 2a). In mid-August, we observed the lowest discharge in the 121 years of monitoring data, 673 m^3/s (yellow dot in Figure 2a). We can define this as a severe drought (below 10th percentile) that lasted for 75 days, highlighted by the yellow shaded area in Figure 2a.

Wind speeds were mainly low and moderate (between 3 and 8 m/s) between June and August. In September and October, there were more frequent occurrences of stronger winds above 10 m/s (Figure 2b), leading to set-up and set-down at the coast (Figure 2d). Onshore winds (northwesterly) can drive an immediate coastal set-up, and a subsequent set-down when the wind relaxes. Alongshore winds can be upwelling-favorable (northeasterly), leading to set-down or downwelling-favorable (southwesterly), resulting in set-up.

There is no clear relationship between tidal range and salt intrusion length. However, there is a clear relation between the spring-neap tidal cycle and stratification (expressed as buoyancy frequency N^2) at the salinity stations along the estuary. Figure S2 in Supporting Information S1 shows a stronger stratification a few days after neap tide, and a weaker stratification a few days after spring tide.

4.2. Stratification Structure

The stratification of the estuary at the beginning of August 2022 is shown in Figure 3, based on shipborne CTD measurements (see ship tracks in Figure 1b). Figure 3a shows the stratification in the Rotterdam Waterway, and Figure 3b shows the stratification in the New Meuse (22–36 km from Hoek van Holland) and the Hollandsche IJssel (36–42 km from Hoek van Holland). In the deeper, overdredged part of the estuary, there is a strongly stratified salt wedge. In the shallow Hollandsche IJssel side branch, the salinity structure is more well mixed, and the horizontal salinity gradient is weaker than in the Rotterdam Waterway and the New Meuse.

4.3. Salt Intrusion Length

Figure 2e shows the evolution of the salt intrusion length in the Lek (L_2), defined as the location of the 2 PSU isohaline. The mean tidal variability is 8.5 km, and the greatest intrusion length was 44.2 km. This occurred on 16 August during a period of very low Rhine discharge of about 700 m^3/s, during a spring tide when there was a small set-up at the coast (Figure 2d). At this time, the tidally averaged intrusion length was 39.9 km. The second largest salt intrusion event occurred in mid-September and had a tidally averaged length of 39.2 km. During this second event, the river discharge was larger than mid-August. However, there had been a prolonged northwesterly wind, leading to an increased wind set-up at the coast (see Figures 2b–2d). The set-down afterward also rapidly decreased the salt intrusion length. More events will be examined in Section 4.5. During the period of low discharge without major set-up events, for example, between the 6th and the 15th of August, the landward propagation of the salt front was approximately 0.86 km/day. For the most extreme set-up event, the upstream propagation speed was 4.32 km/day.

4.4. The Role of River Discharge

The relation between the 5-day mean of the Rhine River discharge and the 5-day mean of the salt intrusion length L_2 is shown in Figure 4a. Following a power law relation between river discharge Q_R and salt intrusion length $L_2 \propto Q_R^{-n}$, the observed values give the best fit for $n = 0.35 \pm 0.03$. This is larger than values found for other salt wedge estuaries, for example, $n = 0.2$ in the Duwamish River Estuary (McKeon et al., 2021) and $n = 0.19$ in the Merrimack River Estuary (Ralston et al., 2010) for low discharge. For 5-day means, the Rhine River discharge explains $88 \pm 5\%$ of the variance in intrusion length, but only $69 \pm 3\%$ of the variance for tidal means. Most of the outliers of the tidal means can be explained by variability due to coastal set-up. The dependence of anomalies in the discharge relationship on coastal set-up is shown in Figure S1 in Supporting Information S1. Storm surge

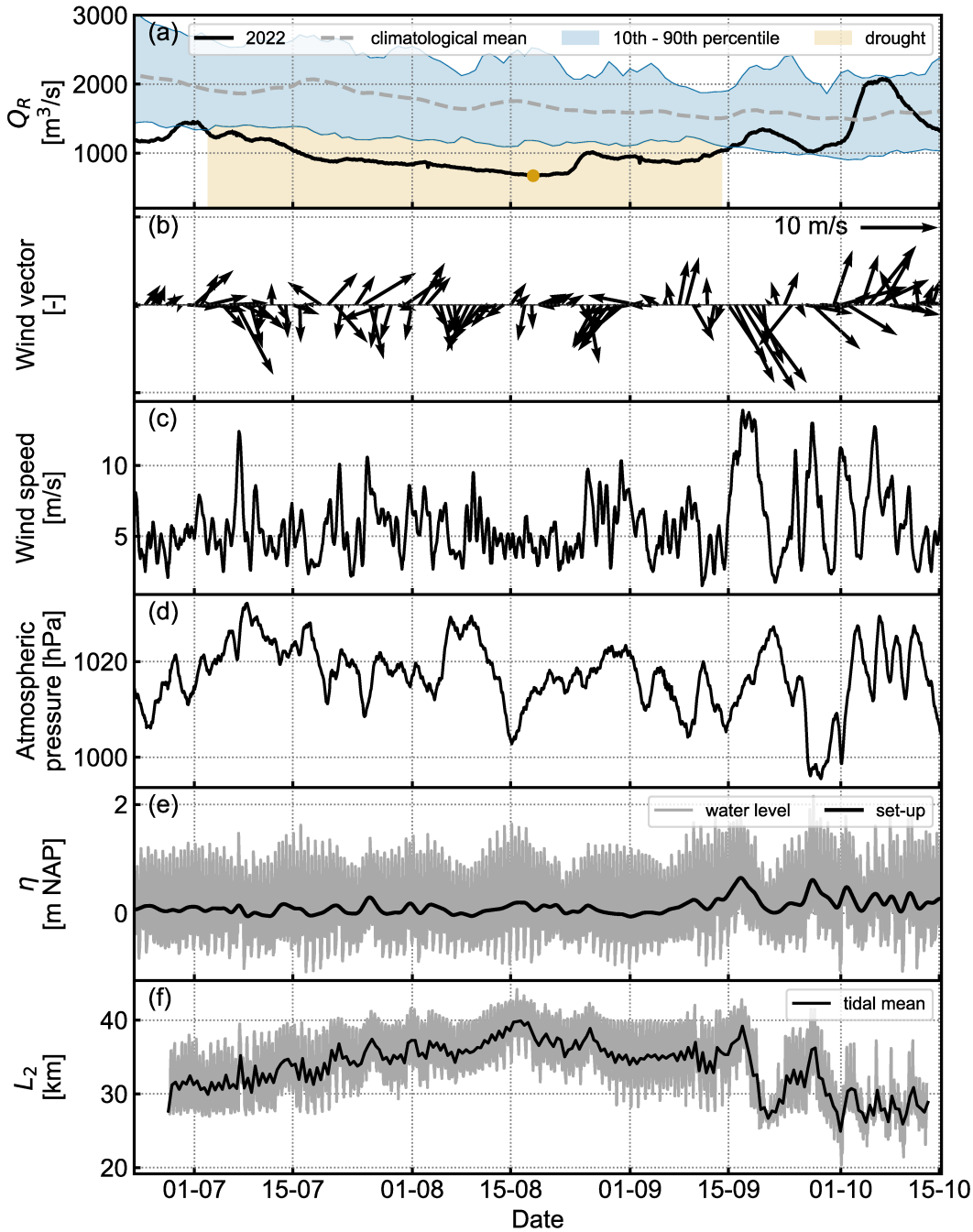

Figure 2. Forcing conditions and salt intrusion length between 13 June and 25 October 2022, including (a) the Rhine River discharge Q_R (m^3/s), showing the mean and 10th–90th percentile range for the climatological period (1992–2021) and the period of severe drought, (b) the wind vector, (c) wind speed (m/s), and (d) atmospheric pressure at sea level (hPa) at Hoek van Holland, (e) the measured water level η and calculated set-up $\langle\eta\rangle$ (meters NAP) at Hoek van Holland, and (f) the salt intrusion length L_2 in the Lek (km), defined as the 2 PSU isohaline.

events act on a timescale of 1.5–6 days, which are mostly averaged out by a 5-day mean. The dependence of salt intrusion on coastal set-up is further discussed in subsection 4.5.

We show the salinity at Brienenoordbrug and the Rhine River discharge between 1978 and 2022 for the summer months June, July, and August (JJA) in Figure 4b. The data points of the field campaign of 2022 are represented by blue circles. Most of the data points of 2022 are located in the yellow shaded area, representing high salinity

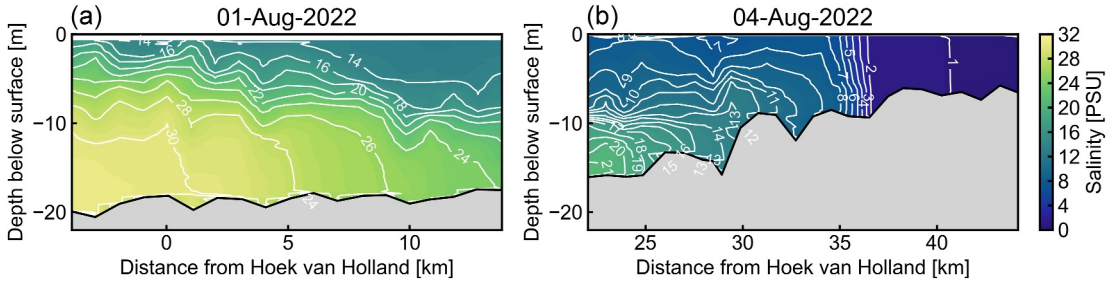

Figure 3. Along-channel salinity structure on flood tide (a) in the Rotterdam Waterway on the 1st of August 2022 and (b) in the New Meuse (22–36 km) and Hollandsche IJssel (36–42 km) on the 4th of August 2022.

and low discharge, defined as severe drought conditions or worse ($Q_R < 1180$ m^3/s, below 10th percentile). There is no power law dependence in the high discharge tail ($Q_R > 2000$ m^3/s). For high discharges, the salinity at Brienenoordbrug reaches the background chloride concentration of the fresh river water, and the salt intrusion length does not reach beyond the observation point. This background salinity concentration S is dependent on the amount of discharge with $S = a/Q_R + b$ (van der Weijden & Middelburg, 1989), where a is the chloride load and b the base chloride concentration, that is, a constant background concentration. For the summer months between 1992 and 2022, we found $S_{Lobith} = 100.58 \cdot Q_{Lobith}^{-1} + 0.094$, indicated by the dashed line in Figure 4b. To show how exceptional the salinity levels recorded in 2022 were, we ranked the 5-day average salinity concentration since 1,978 and found that 35 of the top 100 records occurred in 2022.

4.5. The Role of Wind and Atmospheric Forcing

Atmospheric forcing drives changes in atmospheric pressure, local wind, and remote wind. Variations in coastal set-up can be driven by changes in wind conditions and atmospheric pressure (Figure 2). Atmospheric pressure drives variations in water level due to the inverted barometric effect (Dangendorf et al., 2014; Wunsch & Stammer, 1997). To evaluate the influence of coastal set-up on salt intrusion, we consider the subtidal water level at Hoek van Holland.

Estuaries are most susceptible to salt intrusion during periods of low discharge, and the corresponding dependency for the Rhine-Meuse Delta is shown in Figure 4a. The coastal set-up can cause perturbations landward or seaward from the expected location for a given discharge, as shown by the tidal averages in Figure 4a. Because the effect of coastal set-up on salt intrusion occurs over timescales of a few days, its importance is best shown by its influence on the speed of the intrusion (s_1 in Equation 1). Figure 5 shows the dependence of the salinity

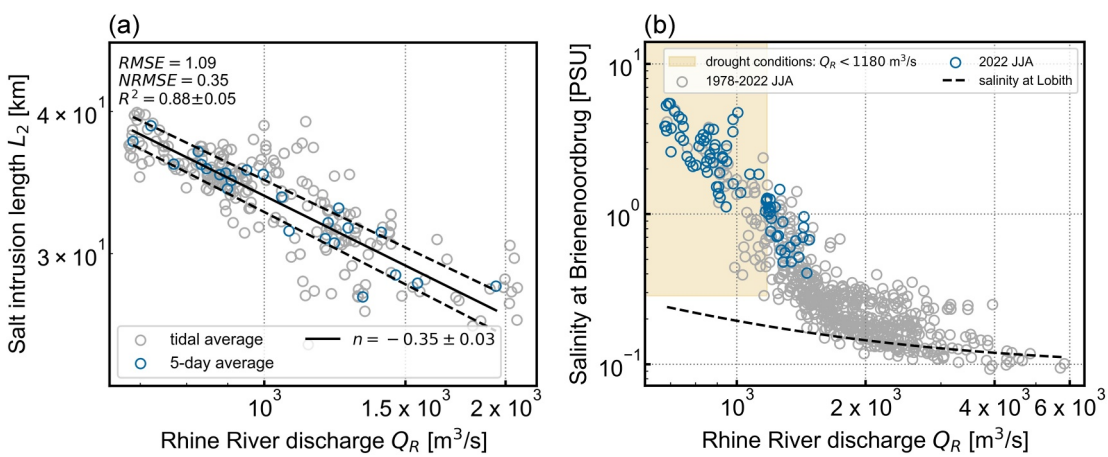

Figure 4. Discharge dependence of salinity: (a) Rhine River discharge Q_R (m^3/s) versus salt intrusion length L_2 (km) for 5-day-averaged values in blue and tidal averages in gray; the solid black line indicates the least squares power law fit, and the dashed lines indicate this fit $\pm RMSE$. (b) Rhine River discharge Q_R (m^3/s) versus salinity (PSU) at Brienenoordburg, 35 km from the mouth between 1978 and 2022 for 5-day-averaged values of the summer months (June, July, and August). The yellow shaded area highlights severe and worse droughts (below 10th percentile); the dashed line indicates the calculated river salinity concentration at Lobith based on the discharge.

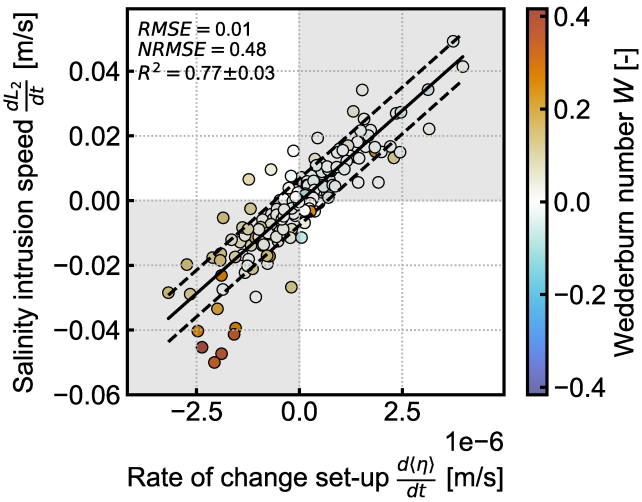

Figure 5. Coastal set-up dependence of salt intrusion length, showing the tidally averaged rate of change of subtidal water level at Hoek van Holland $\frac{d\langle\eta\rangle}{dt}$ (m/s) versus salinity intrusion speed $\frac{dL_2}{dt}$ (m/s), The black line indicates the least squares linear fit, and the dashed lines indicate this fit $\pm RMSE$; the colors indicate the dimensionless Wedderburn number W; see Equation 2.

intrusion speed $\frac{dL_2}{dt}$ (m/s) on the rate of change of the subtidal water level at the mouth $\frac{d\langle\eta\rangle}{dt}$ (m/s). Here, positive intrusion speed represents landward movement. The gradients were based on low-pass filtered time series with time steps of 10 min. There is a strong correlation between those quantities, especially for increasing coastal set-up. The intrusion speed correlates with the rate of change of set-up, because those variations in coastal set-up can drive a volume flux of ocean water up-estuary, as the water levels in the estuary adjust to the offshore water level Wong and Valle-Levinson (2002). These results indicate that the set-up is not a general predictor of the salt intrusion length but drives changes in the salt intrusion length on shorter timescales (1.5–6 days).

To describe the effect of local, along-estuary (northeasterly) winds on salt intrusion, we evaluate the Wedderburn number W, a dimensionless number, defined as the ratio between the along-channel wind stress and the along-channel baroclinic pressure gradient (Geyer, 1997)

$$W = \frac{\tau_w L}{\Delta\rho g H^2}, \tag{2}$$

with along-channel wind stress (up-estuary is taken positive here) τ_w, salt intrusion length L, the density difference between the mouth and the location of the salt intrusion limit $\Delta\rho$, gravitational acceleration g, and depth of the surface layer H. Wind stress can be estimated by $\tau_w = C_d\rho_a U_{10}|U_{10}|$, with the wind speed 10 m above the surface U_{10}, the density of air $\rho_a = 1.2$ kg/m^3, and the dimensionless drag coefficient $C_d = 0.0015$ (Wilson, 1960). By means of the ship surveys, we estimated the surface layer depth to be 8 m (Figure 3a).

We found the primary driver of salt intrusion related to wind to be $\frac{d\langle\eta\rangle}{dt}$, and therefore colored the dots in Figure 5 by their value of W. The outliers below the RMSE in the relation between $\frac{dL_2}{dt}$ and $\frac{d\langle\eta\rangle}{dt}$ (Figure 5) are associated with the highest values of $W \approx 0.4$, and correspond to a decreasing mean water level. These outliers correspond to the wind events on the 17th of September and the 27th of September (see the first two yellow highlighted events in Figure 6). For high W, the transport by estuarine circulation is reduced, which could result in a faster retreat of the salt intrusion, than the rate of change that is predicted by the fit of the data, based on the occurring set-down.

We further analyze the relation between L_2 and $\langle\eta\rangle$ by selecting the wind events above 0.15 m NAP (Figures 6a and 6b). Those set-up events are indicated with blue dots for the maxima and green dots for minima in the set-up time series (Figure 6a) and salt intrusion length time series (Figure 6b). The maximum time lag between the maxima in set-up and salt intrusion length is 25 hr, and the mean is approximately 9 hr. Within one event, L_2 can move up to 6.2 km upstream and up to 12.5 km downstream. This movement is approximately equal to the tidal excursion length, which is estimated to be 8.5 km. In most of the events, the increase in salt intrusion length during the set-up differs from the retreat in salt intrusion length during the set-down. In 11 of the 13 cases, the larger increase in salt intrusion than the decrease in salt intrusion corresponds to a larger set-up than set-down subtidal water level change, and vice versa. During these events, L_2 reaches a maximum event-averaged speed of 0.086 m/s, which is roughly twice the average freshwater flow speed in the New Meuse in summer.

We examine representative wind and set-up-driven salt intrusion events that occurred between the 17th of September and 10th October; these are highlighted in yellow in Figure 6. Two days of persistent strong onshore (northwesterly) winds preceded the salt intrusion event on September 17th (Figures 6c–6h). During these days, the coastal set-up at Hoek van Holland increased to 0.65 m above NAP. The time lag between the maximum intrusion event of 39.2 km and the maximum set-up was approximately 4 hr. The intrusion length before the event was about 35.0 km. After the peak water levels and peak salt intrusion length, the subsequent set-down drove a downstream propagation of the salt front of 12.6 km, so it became shorter than before the intrusion event, namely 26.7 km. This relatively large decrease in intrusion length during the set-down can be explained by the strong up-estuary (also onshore) wind speed. These days had the largest observed Wedderburn number values (red dots in

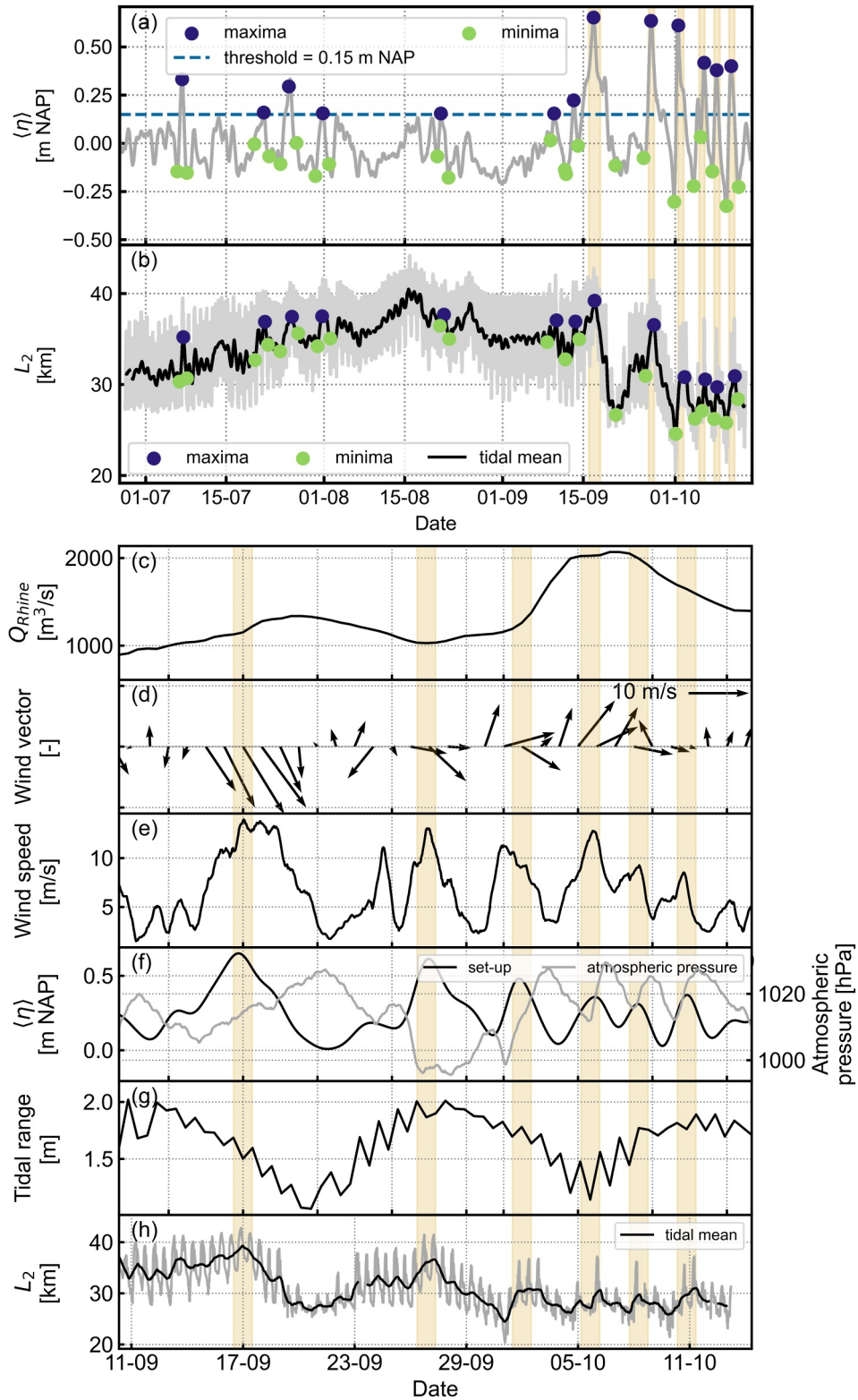

Figure 6. Overview of the selected coastal set-up events, including (a) coastal set-up at Hoek van Holland $\langle\eta\rangle$ (meters above NAP) and (b) salt intrusion length L_2 (km). The yellow highlighted events are zoomed in upon with additional parameters. (c) Rhine River discharge Q_{Rhine} (m^3/s). (d) The daily mean wind vector. (e) $\langle\eta\rangle$ (meters NAP) and atmospheric pressure (hPa) at Hoek van Holland. (f) The tidal range (m) at Hoek van Holland. (g) L_2 (km). The yellow areas highlight 48 hr around the maximum set-up.

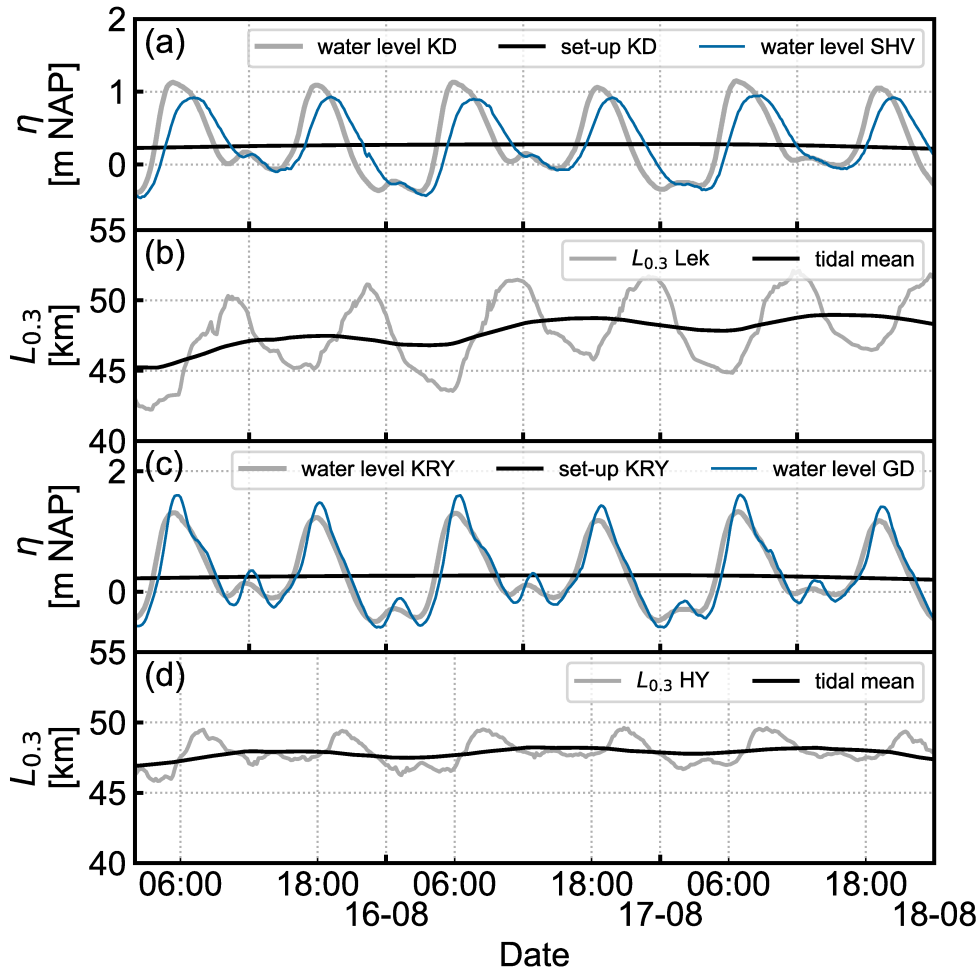

Figure 7. The time series of (a), (c) water level η (m NAP) at the mouth and upstream control of the river branch and (b), (d) salt intrusion length $L_{0.3}$ (km). Here panels (a) and (b) correspond to the Lek branch, and panels (c) and (d) to the Hollandsche IJssel branch.

Figure 5), which indicates that the salt import by the gravitation circulation decreased during these days. Furthermore, the Rhine River discharge increased during this event as well.

In October, we observed a series of salt intrusion events driven by coastal set-up. The time series in Figure 6e and f show that fluctuations in wind speed and atmospheric pressure are in phase with the coastal set-up. The wind speed has a positive correlation and the atmospheric pressure has a negative correlation with set-up. Figure 6d shows that most of the time we observed direct onshore (northwesterly) winds or downwelling (southwesterly) winds. Both onshore and downwelling winds can drive a set-up at the coast. The longest tidally averaged intrusion length was 36.6 km, and the maximum set-up was 0.64 m. The time lag between the set-up peaks and salt intrusion peaks varied from 2 to 26 hr.

4.6. Side Branches

In this section, the Lek and the Hollandsche IJssel are studied in more detail, because the dynamics in those branches differ from the main river stem (Kranenburg et al., 2022). Those differences are mainly caused by their geometry and because local water management has a bigger impact. They can be thought of as subestuaries within the larger delta channel network.

As a result of the difference in length between the two branches, tidal flows in the branches have a different phasing with respect to flow velocity to the New Meuse. The Hollandsche IJssel is shorter than the Lek and has a standing tidal wave, whereas the main channel and the Lek have a propagating tidal wave. Figure 7c shows that

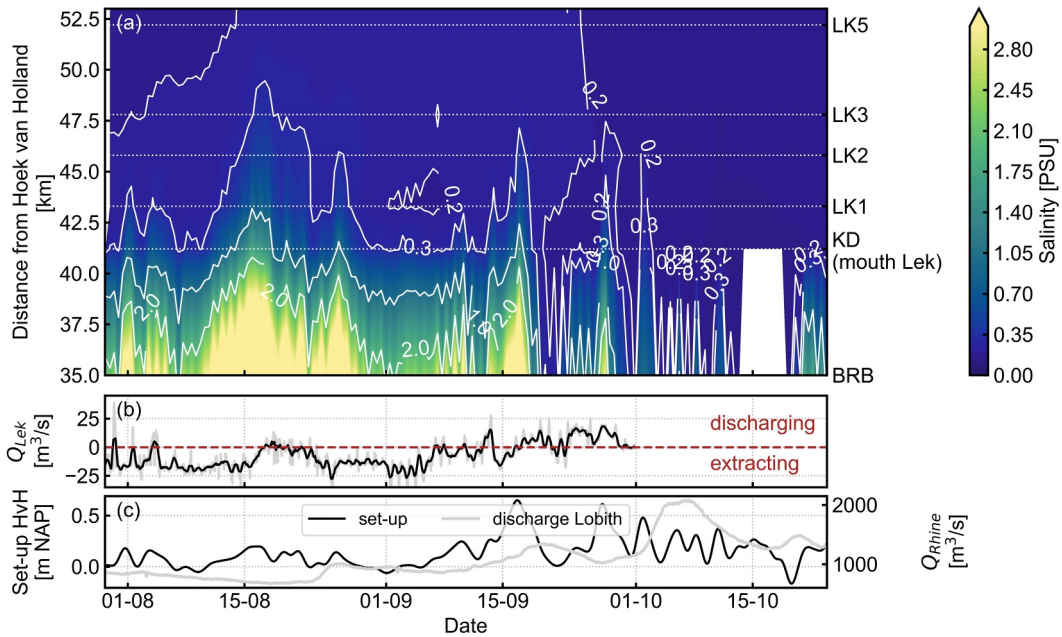

Figure 8. (a) Salinity contours (PSU) in the New Meuse and Lek, between salinity stations BRB and LK5. The salinity values are interpolated between the stations, whose locations are indicated by white dotted lines. (b) Discharge through the Lek Q_{Lek} (m^3/s), where positive values represent a net freshwater discharge on the Lek and negative values net extractions from the Lek. (c) Set-up $\langle\eta\rangle$ (m NAP) at Hoek van Holland and Rhine River discharge Q_{Rhine} (m^3/s).

the water level at Gouda and KRY are in phase, which indicates a standing wave. Contrastingly, the phase difference between water levels at KRY and SHV indicates a propagating tidal wave in the Lek (Figure 7a). The main channel has a phase difference in flow velocity of 55° with the Hollandsche IJssel and 31° with the Lek (de Wilde, 2024). As a result, the Hollandsche IJssel has ebb flow for a long time when the main channel is flooding.

To further evaluate the difference in dynamics, we look at the evolution of the tidally averaged salinity contours together with the discharge through the branch, the set-up at Hoek van Holland, and the Rhine River discharge for the two different river branches in Figures 8 and 9. The discharge through the branches is human-controlled and consists of a summation of inlets and discharging stations. At those stations, freshwater can be extracted from or discharged into the branch. Figures 8b and 9b indicate whether there is a net extraction ($Q_{branch} < 0$ m^3/s) or a net discharge ($Q_{branch} > 0$ m^3/s) in the branch.

The longest tidally averaged intrusion lengths $L_{0.3}$ in the two branches were observed in different months. In the Lek, an intrusion length $L_{0.3}$ of 48.6 km occurred on the 17th of August. In the Hollandsche IJssel, a salt intrusion length of 50.5 km was observed a month later, on the 24th of September.

In the Lek, $L_{0.3}$ follows a temporal pattern closely related to the salinity at its mouth (41 km), see Figure 8. Roughly between 7th and 15th August, there is a net negative discharge, the set-up at Hoek van Holland is slightly decreasing, and the Rhine River discharge is decreasing. This results in increasing salinities in the Lek, where a peak is reached on August 17th. On August 15th, the weir at Hagestein (upstream control of the Lek) was opened to flush out saline water from the branch. This increased net discharge ($Q_{Lek} > 0$ m^3/s), combined with a slight set-down, which decreases salinity at the Lek mouth, reduced the salt intrusion length. Later, we also observe a strong response of the salt intrusion in the branch to the set-up at Hoek van Holland. The clearest examples occur around 17th and 26th September when the Rhine discharge is still around 1,000 m^3/s.

Interestingly, $L_{0.3}$ of the Hollandsche IJssel shows less correlation with the salinity at the mouth of the branch. The low salinity limit does not follow a similar pattern as the salinity at the mouth of the branch (36 km). The value of $L_{0.3}$ remains between 46 and 48 km from 14th August up to the 17th of September. Between 6th and 10th of September, there is a slight increase in discharge through the branch, with a corresponding decrease in salt intrusion length. This decrease in $L_{0.3}$ is followed by an increase due to the set-up event around the 16th of

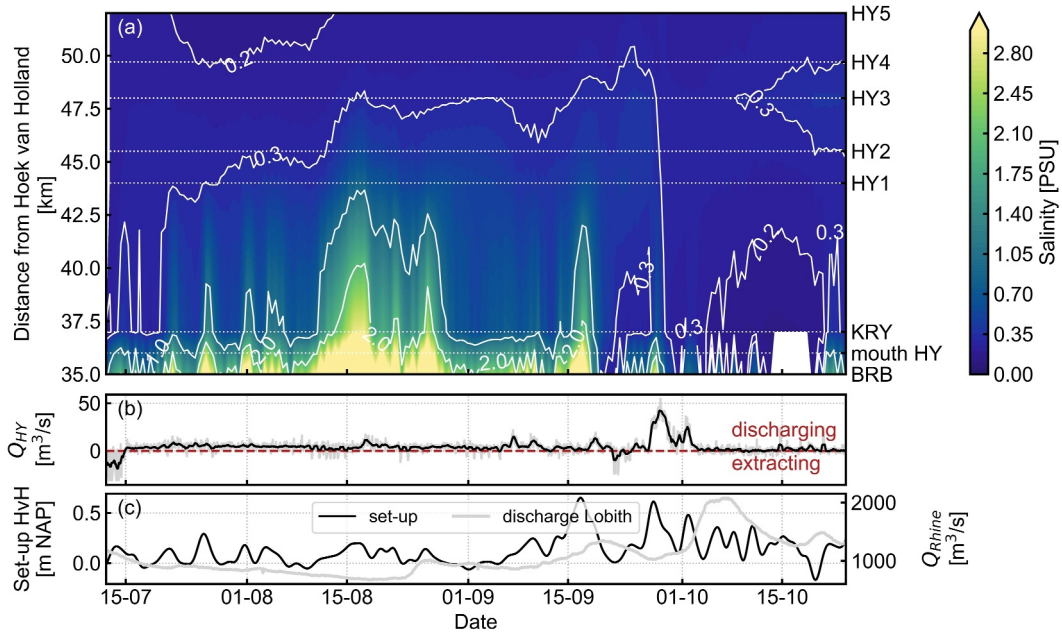

Figure 9. (a) Salinity contours (PSU) in the New Meuse and Hollandsche IJssel, between salinity stations BRB and HY5. The salinity values are interpolated between the stations, whose locations are indicated by white dotted lines. (b) Discharge through the Hollandsche IJssel Q_{HY} (m^3/s), where positive values represent a net freshwater discharge on the Hollandsche IJssel (HY) and negative values, net extractions from the Hollandsche IJssel. (c) Set-up $\langle\eta\rangle$ (m NAP) at Hoek van Holland and Rhine River discharge Q_{Rhine} (m^3/s).

September. L_2, which is located around the mouth of the Hollandsche IJssel during this period, propagates upstream and downstream with the corresponding set-up and set-down. However, there is no strong response of $L_{0.3}$ to the set-down. The reduction in salinity intrusion length $L_{0.3}$ started only after September 26th, coinciding with a significant increase in discharge from the Hollandsche IJssel. This increase in discharge coincides with a strong set-up at Hoek van Holland, which eventually flushes out all salinity above 0.3 PSU on the subsequent set-down. The set-up events in October, associated with up-estuary salt transport, drive $L_{0.3}$ into the branch again. However, there are no major intrusions anymore, since the Rhine discharge has started to increase again.

The difference in the evolution of $L_{0.3}$ between the two branches is caused by the tidal phase difference between the two branches. The Hollandsche IJssel has an earlier flow reversal; therefore, there is ebb flow in the branch while the New Meuse is at the end of flood tide, with corresponding high salinity concentrations. This is shown in Figure 7b and d by the small intratidal variability in salt intrusion length compared to the Lek. Once the Hollandsche IJssel becomes saline, the salt concentrations stay in the branch for a relatively long time (Figure 9a).

Unlike in the main branch, the salt intrusion length in the side branches is most strongly correlated with downstream salinity in the main stem, which is at Brienenoordbrug (35 km) (Figure 10), rather than discharge through the branch (Figure S3 in Supporting Information S1). Here, we evaluated 3-day averages for salinity and salt intrusion, to consider the estimated average response times. The estimated response times $T_{ADJ} = \frac{1}{2}\frac{L_s}{u}$ (Lerczak et al., 2009; MacCready, 2007) for the Lek branch was 3–4 days, and for the Hollandsche IJssel, it was 15 days. The stronger dependence on downstream salinity than other factors is due to a combination of significant salinity changes at the downstream boundary and a weak horizontal salinity gradient in the branches. At Brienenoordbrug, the tidal average salinity varies between 0 and 6 PSU, so the salinity varies over more than an order of magnitude, whereas the salinity at the mouth of the main system is expected to vary with only roughly 10% (Y. Lee & Lwiza, 2008; Schloen et al., 2017; Salcedo-Castro et al., 2023). When the downstream salinity increases, the horizontal salinity gradient increases, and the tidal dispersion term also increases. We consider the downstream salinity as a separate forcing because the side branches are decoupled from this downstream end; they have different tidal phasing and discharge compared to the main branch.

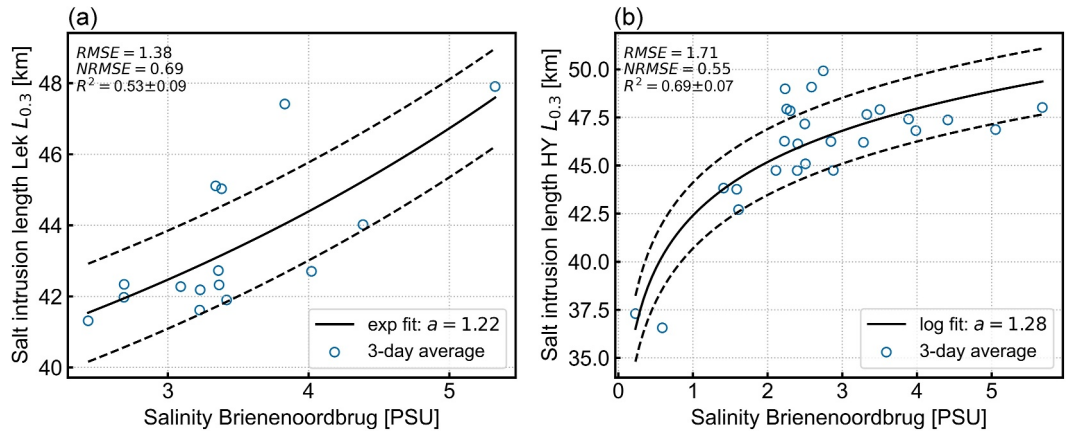

Figure 10. Salt intrusion length $L_{0.3}$ (km) versus salinity at the nearest downstream station, Brienenoordbrug, 35 km from Hoek van Holland (PSU) for 3-day averages (a) in the Lek and (b) in the Hollandsche IJssel (HY). The black line indicates the empirical least squares fit and the dashed lines $\pm RMSE$ of this fit.

However, two other important forcing mechanisms act on shorter timescales, thus influencing the salinity intrusion speed. For the Hollandsche IJssel, the net discharge through the branch explains 49% of the variance and is a good predictor for the rate of change of salt intrusion (Figure 11b). In the Lek, the rate of change of salt intrusion is more dependent on the rate of change of set-up at the mouth (Figures 11a and 11c), which explains 60% of the variance. The relation between salt intrusion speed and discharge in the Lek (Figure 11a) contains many outliers, where the high outliers correspond to a strongly increasing subtidal water level and the low outliers correspond to a strongly decreasing subtidal water level. Similarly, in the relation between the rate of change of set-up and the salinity intrusion speed of the Hollandsche IJssel, the high outliers correspond to low net discharges in the Hollandsche IJssel, and low outliers to high net discharges.

The effect of the discharge can be explained by 'sucking and flushing', where the saline water is sucked in during periods of negative discharge (lower left shaded area in Figures 11a and 11b), and flushed out for positive net discharges (upper right shaded area in Figures 11a and 11b). Here, the rate of change of salinity intrusion speed scales with the freshwater flow velocity u_R as $\frac{dL}{dt} \propto -Q_{branch}/A$, with the cross-sectional area of the river A. This relation was confirmed for the Hollandsche IJssel for another period as well (Kuijper, 2016). We can explain this relation by looking at the balance of the terms by considering the depth-averaged, tidally averaged, salt conservation balance (Equation 1), which we introduced in Section 2.

The observed balance between the unsteadiness term and advection by river discharge can hold when changes in river discharge have a negligible effect on the exchange flow term. In this case, the exchange flow term s_3 should become negligible relative to the diffusion term s_4, and the balance in Equation 1 then reduces to an advection-diffusion equation. When $s_4 \ll s_2$, the scaling between discharge and salt intrusion length is only found in terms s_1 and s_2, which gives $\frac{dL}{dt} \propto -\frac{Q}{A}$. Due to the occurrence of negative discharges, s_2 can be both positive and negative in the side branches. Therefore, the balance between s_1 and s_2 can hold here for a longer time than regular estuaries, where s_2 only results in salt export by river flow.

5. Discussion

We studied salt intrusion during low discharge conditions, when estuaries are most susceptible to salt intrusion events. The Rhine-Meuse Delta shows a power law relation between salt intrusion length and discharge for 5-day averages. On shorter timescales (e.g., a couple of tidal cycles), coastal set-up drives fluctuations comparable to the tidal excursion length. However, tides do not appear to affect the subtidal salt intrusion. Conversely, in the side branches with a human-controlled discharge, the primary driver of the salt intrusion length was downstream salinity. This is different from most estuaries studied because ocean salinity at the estuary mouth is usually relatively constant. On shorter timescales, shown by the dependence on salinity intrusion speed, the coastal set-up and discharge played a role in determining salt intrusion dynamics.

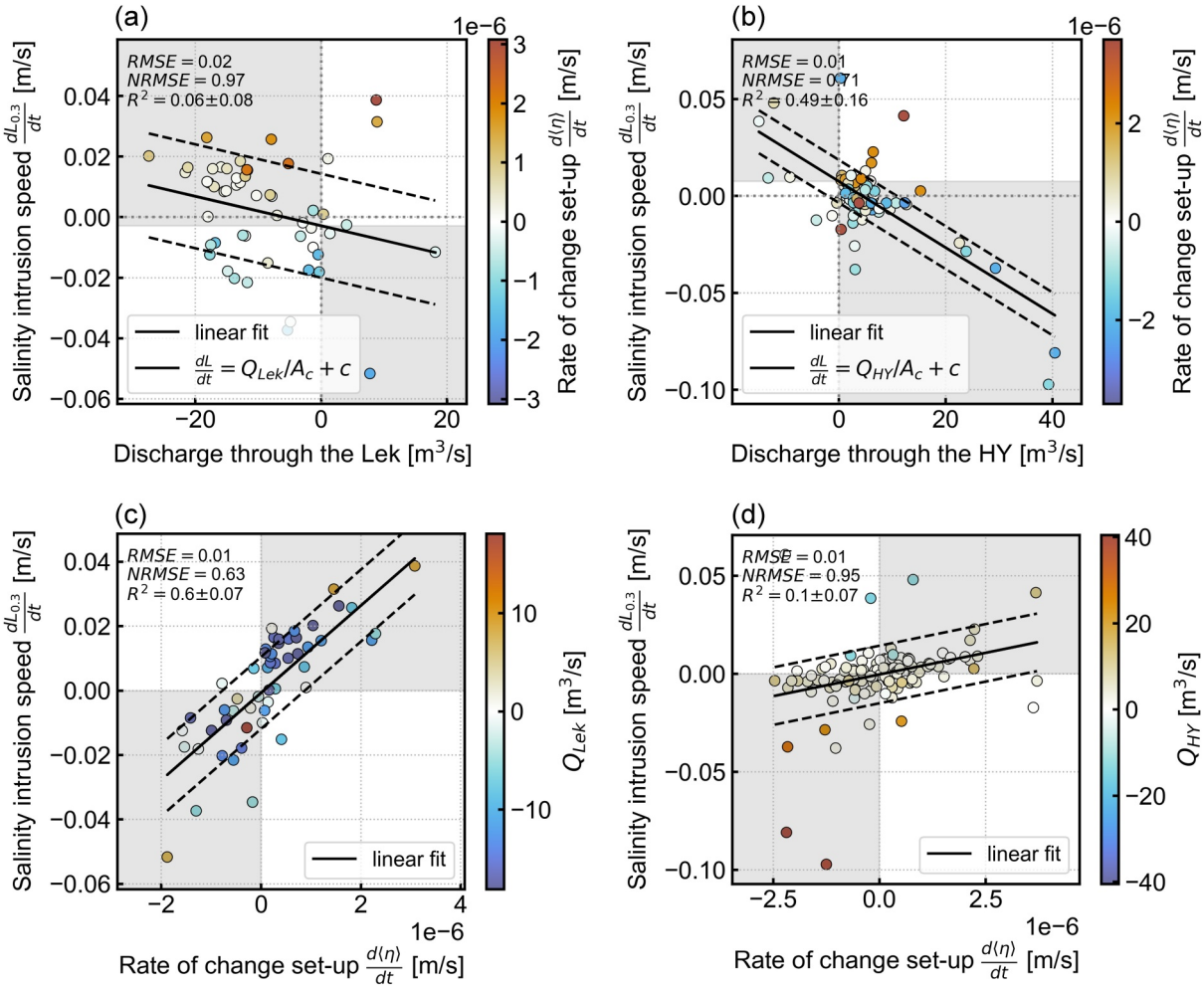

Figure 11. Salinity intrusion speed of $L_{0.3}$ versus discharge through the mouth of the river branch Q_{branch} (m^3/s) (a), (b) and on rate of change of set-up $\frac{d\langle\eta\rangle}{dt}$ (m/s) (c), (d) in the Lek branch (left column) and Hollandsche IJssel branch (right column). In (a) and (b) the colors of the dots indicate the rate of change of set-up at Hoek van Holland. In (c) and (d) the colors of the dots indicate the discharge through the branch. The black lines indicate the least squares linear fit and the dashed lines this fit $\pm RMSE$. The gray areas represent the offset from zero salinity intrusion speed.

Here, we show a power law relation between salt intrusion length and discharge with an exponent of $n = 0.35 \pm 0.03$. Close values can be found for both salt wedge estuaries, for example, the Merrimack and the Duwamish $n \approx 0.2$ (McKeon et al., 2021; Ralston et al., 2010) and partially to well-mixed estuaries, for instance, the Delaware Bay and Hudson River estuary $n \approx 0.3 - 0.4$ (Abood, 1974; Cook et al., 2023). Theoretical models predict exponents of $n = 1/3$ for estuaries dominated by exchange flow (e.g., Hansen and Rattray (1965); MacCready (2004)), $n = 1$ for estuaries dominated by tidal salt fluxes (Lerczak et al., 2009; MacCready, 2007), and $n = 2$ for arrested salt wedges (Schijf & Schönfeld, 1953). However, results from field observations often differ due to factors like unsteadiness and the presence of branching channel networks (Conroy et al., 2020), and along-estuary bathymetry variation (Ralston et al., 2008). Furthermore, Poggioli and Horner-Devine (2015) showed that a sloping bottom and channel convergence reduced the expected exponent for salt wedge estuaries. This exponent highlights the sensitivity of the estuary to changes in river discharge and the relative importance of other processes. In the Rhine-Meuse Delta, the observed value suggests that additional factors, such as unsteadiness from coastal set-up and the complex channel system, also play a significant role.

Unlike the main system, the relation between salt intrusion in the side branches and their discharge does not follow a power law. In the side branches, there is no steady-state balance with the discharge, but discharge drives variations on shorter timescales, which impacts the salinity intrusion speed. The salt balance is dominated by unsteadiness and advection, which means the relation between salt intrusion and discharge is described by

$\frac{dL_{0.3}}{dt} \propto -\frac{Q}{A}$. This holds when the exchange flow term (s_3 in Equation 1) is small. In the side branches, the exchange flow is expected to be weak, because the horizontal salinity gradient $\frac{\partial \bar{s}}{\partial x}$ is weak, as there is a weak vertical stratification, and the side branches are shallower than the main system (Figure 3). The unsteadiness term is expected to be relatively important here because there are many sudden changes in discharge. The sudden changes in discharges in the branches happen because they are determined by extraction locations, rather than a natural river basin source, as in the main branch. For unmanaged estuaries, this balance cannot hold for a long time because sudden increases in discharge would flush out most of the saline waters. In this highly managed system, this balance can persist for a longer time, because the river advection can become a source of salt import, due to the negative discharges.

Another difference between the main branch and the side branches was the importance of downstream salinity variation for salt intrusion length in the side branches. This importance could be attributed to the small salinity gradient in these regions, along with the potential importance of the tidal dispersion and advection terms relative to the estuarine exchange term. When the salinity at the mouth of the side branches doubles, the along-channel salinity gradient, and subsequently, the tidal dispersion flux doubles. We assume this is one of the dominant terms; therefore, the intrusion length responds strongly. For most estuaries, the variability in salinity at the mouth, due to upwelling or seasonal trends is relatively minor, generally within a few PSU (around 5%–10% of an approximate of 30 PSU) (Y. Lee & Lwiza, 2008; Schloen et al., 2017; Salcedo-Castro et al., 2023). In contrast, the branches of the estuary experience much greater salinity variation, often exceeding 100% relative to their mean values. Consequently, regular changes in sea salinity could not impact the horizontal salinity gradient, and subsequent change in salt intrusion length as much as they can in the side branches. For multiple-channel systems, however, the ocean boundary can be more variable, due to the presence of several freshwater sources (e.g., Zhang et al. (2012); Korotenko et al. (2014)).

Similar to many observations in estuaries (e.g., Wong and Garvine (1984); de Nijs et al. (2008); Zhu et al. (2020); Eslami, Hoekstra, Kernkamp, et al. (2021); Cook et al. (2023)), we found a strong relation between coastal set-up and salinity in the estuary. Wong and Valle-Levinson (2002) showed that the up-estuary volume flux Q_{in} associated with the changing subtidal water level can be estimated by $Q_{in} = \frac{\partial \langle \eta \rangle}{\partial t} A_s$ in Chesapeake Bay. Here, $\langle \eta \rangle$ is the subtidal water level and A_s is the surface area of the estuary. We showed that the rate of change of the salt intrusion length also scales with $\frac{\partial \langle \eta \rangle}{\partial t}$ in the Rhine-Meuse Delta estuary. This strong response to salt intrusion suggests the presence of a strong landward salt transport during coastal set-up events, which was seen in some numerical studies of the Rhine-Meuse Delta (Cox et al., 2021; Kranenburg et al., 2022).

While the effect of coastal set-up on salt intrusion is evident throughout the measurement campaign, the influence of along-estuary winds is only clear for the highest observed Wedderburn numbers around 0.4, which occurred during two wind events. Along-estuary winds were found to be important in several estuaries (Cook et al., 2023; Geyer, 1997; Scully et al., 2005). In deeper systems like the Delaware River Estuary (Cook et al., 2023) and the Rhine-Meuse Delta estuary, high wind speeds are necessary to generate a response, as opposed to the shallow estuaries in Waquoit Bay, Cape Cod, described by Geyer (1997).

Similar to our observations in the Rotterdam Waterway, many estuaries have a distinct spring-neap variation in stratification (e.g., Lewis and Lewis (1983); Stacey et al. (2001); Jay and Dungan Smith (1990); Bowen and Geyer (2003); Giddings et al. (2011)), as well as a spring-neap variability in the strength of gravitation circulation (Eslami, Hoekstra, Kernkamp, et al., 2021). This variability could be attributed to the amount of mixing (Geyer et al., 2000; Lerczak et al., 2006). However, no correlation was found between the tidal range and salt intrusion length in the Rhine-Meuse Delta estuary. This could be due to a large response time that increases during low river discharge, as was observed in the Hudson River Estuary (Bowen & Geyer, 2003; Lerczak et al., 2009). The estimated response times for the main system and the Lek branch are 3–4 days, and for the Hollandsche IJssel, it was approximately 15 days. With these response timescales, it is possible that the salt intrusion length cannot fully adjust to the changing tidal velocities within a spring-neap cycle. Another explanation could be that both the salt flux due to estuarine circulation and the salt flux by tidal dispersion processes vary on a fortnightly timescale. Fluxes by estuarine exchange flow are expected to be at a maximum around neap tides and a minimum around spring tides, whereas it is the other way around for the tidal dispersion processes. If the salt fluxes from these mechanisms are of similar magnitude, their net effect on the total salt flux and the resulting spring-neap variations

in salt intrusion length will be negligible. This is consistent with a recent numerical study of this system by Huismans et al. (2024).

In the Rhine-Meuse Delta, we observed that discharge is a dominant control of the salt intrusion, both in the main system and the side branches. The power law relation holds best for salinity and discharge values of timescales longer than a single tidal cycle, especially 5-day averages. Set-up, which acts on a shorter timescale is not described in such a balance. However, during drought, elevated salinity levels for a few days can have an impact on freshwater availability. Results of the Rhine-Meuse Delta indicate that adjusting the advection term $\bar{u}\bar{s}$ by substituting $\bar{u} = (Q_R + Q_{in})/A$, similar to Ralston et al. (2008), could be relevant for predictions based on MacCready (2004). This indicates that estuaries with a large surface area A_s are particularly susceptible to coastal set-up-driven salt intrusion. Gerritsma et al. (2024) showed that water levels in the semienclosed Haringvliet also adjust by water that flows through the Rotterdam Waterway, which contributes to the Rhine-Meuse estuary's susceptibility to coastal set-up variations.

River deltas are characterized by a branching channel network with varying channel geometries and bathymetries. This results in a heterogeneous distribution of river discharge and introduces tidal phasing, which are both of major importance for estuarine dynamics. Urban deltas are even more complex because they can exhibit more abrupt depth changes due to dredging activities and independent discharges resulting from flow management. This can lead to very different dynamics in the various branches of the estuary, where different balances dominate. This shows that when studying an integrated operational system for short-term emergency measures during droughts, it is important to be aware that not all branches within the system respond identically to forcing. Through first-order statistical analyses, we showed that treating the side branches separately is crucial in this complex urban delta. While the variability in the downstream salinity boundary is usually not considered in estuaries, we showed the importance of considering this parameter. Treating branches separately is a method to incorporate the downstream boundary condition variability, and may be applied in other deltas or complex estuaries.

6. Conclusions

Using an extensive data set, we analyzed salt intrusion in the Rhine-Meuse Delta during extremely low discharge conditions. Here, the salt intrusion length L_2 follows a strong power law relation with the river discharge with $Q_R^{-0.35 \pm 0.03}$. Coastal set-up modifies this dependence on river discharge, where positive anomalies correspond to set-up, and negative anomalies to set-down. This can be attributed to the up-estuary transport of seawater, which results from the estuary's adjustment to changing water levels at its mouth. The tidal range does not correlate with salt intrusion length. However, there is a relation between tidal range and stratification, which increases during neap tides and decreases during spring tides.

We showed that the overall system dynamics still behave like a simple system, but the side branches must be understood independently. River discharge and coastal set-up determine the overall response of the system, which is relevant because the salinity at the mouth of the upstream branches is the primary predictor for salt intrusion length. Additionally, the localized system dynamics, driven by set-up and discharge through each branch are important, and can differ per branch. Although we have shown that salinity at the mouth mainly drives the salinity intrusion, the relationship to discharge differs significantly from the main branch. A necessary next step is to obtain a more detailed understanding of the behavior of the individual branches.

Understanding salt intrusion dynamics is important in a changing climate. This data set, collected during a severe drought, is crucial for understanding estuaries for which a decreasing discharge and increasing salt intrusion is projected (J. Lee et al., 2024). Besides the important role of discharge, we show that the coastal set-up can drive major fluctuations in salinity intrusion on shorter timescales. Importantly, this means that while discharge is critical for predicting the potential for salinity at upriver locations, coastal set-up may be most important for generating the most severe events during a low discharge period. The dynamics in the side branches can be very different from the main river branch; this indicates that potential different dynamics in side branches have to be well understood and validated to perform high-resolution predictions.

Data Availability Statement

Data from permanent monitoring stations of water level, discharge, and salinity can be retrieved from Rijkswaterstaat (https://www.waterinfo.nl). Meteorological data of wind and atmospheric pressure can be retrieved from the Royal Netherlands Meteorological Institute (https://www.knmi.nl/nederland570nu/klimatologie/uurgegevens). Salinity data collected for this survey are available at 4TU.ResearchData with DOI 10.4121/abc2eb1f-9291-44bd-9810-2ea0e98ae7eb with a CC BY 4.0 license. Discharges in the branches can be requested at the Dutch water boards.

Acknowledgments
This publication is part of the SALTISolutions project with project number P18-32 of the TTW Perspectief programme which is partly financed by the Dutch Research Council (NWO). The authors appreciate the Port of Rotterdam's and Rijkswaterstaat's fieldwork contributions, especially from Arjen Ponger and Jan-Willem Mol. We acknowledge technical support by Pieter van der Gaag, Arie van der Vlies, Arno Doorn, and Chantal Willems from the Hydraulic Engineering Laboratory of TU Delft. We are also thankful for the support of our SALTISolutions and TU Delft colleagues during the fieldwork, including Marlein Geraeds, Daan van Keulen, Floor Bakker, Gijs Hendrickx, Avelon Gerritsma, Bouke Biemond, Wouter Kranenburg, Lennart Keyzer, and Jessamy Mol. Furthermore, we appreciate the collaboration on the processing code with Marlein Geraeds. We are also very grateful to Ymkje Huismans (Deltares and TU Delft) and Nathalie van Veen (Rijkswaterstaat) for the discussions and their willingness to share their knowledge of the system. Finally, we would like to thank two anonymous reviewers for their feedback which substantially improved the manuscript.

References

Abood, K. A. (1974). Circulation in the Hudson estuary. *Annals of the New York Academy of Sciences*, *250*(1), 39–111. https://doi.org/10.1111/j.1749-6632.1974.tb43895.x

Alebregtse, N., & de Swart, H. (2016). Effect of river discharge and geometry on tides and net water transport in an estuarine network, an idealized model applied to the Yangtze Estuary. *Continental Shelf Research*, *123*, 29–49. https://doi.org/10.1016/j.csr.2016.03.028

Bowen, M. M., & Geyer, W. R. (2003). Salt transport and the time-dependent salt balance of a partially stratified estuary. *Journal of Geophysical Research*, *108*(C5). https://doi.org/10.1029/2001JC001231

Chatwin, P. (1976). Some remarks on the maintenance of the salinity distribution in estuaries. *Estuarine and Coastal Marine Science*, *4*(5), 555–566. https://doi.org/10.1016/0302-3524(76)90030-X

Chawla, A., Jay, D. A., Baptista, A. M., Wilkin, M., & Seaton, C. (2008). Seasonal variability and estuary-shelf interactions in circulation dynamics of a river-dominated estuary. *Estuaries and Coasts*, *31*(2), 269–288. https://doi.org/10.1007/s12237-007-9022-7

Conroy, T., Sutherland, D. A., & Ralston, D. K. (2020). Estuarine exchange flow variability in a seasonal, segmented estuary. *Journal of Physical Oceanography*, *50*(3), 595–613. https://doi.org/10.1175/JPO-D-19-0108.1

Cook, S. E., Warner, J. C., & Russell, K. L. (2023). A numerical investigation of the mechanisms controlling salt intrusion in the Delaware Bay estuary. *Estuarine, Coastal and Shelf Science*, *283*, 108257. https://doi.org/10.1016/j.ecss.2023.108257

Cox, J. R., Huismans, Y., Knaake, S. M., Leuven, J. R. F. W., Vellinga, N. E., van der Vegt, M., et al. (2021). Anthropogenic effects on the contemporary sediment budget of the lower rhine-meuse delta channel network. *Earth's Future*, *9*(7), e2020EF001869. https://doi.org/10.1029/2020EF001869

Dai, Z., Chu, A., Stive, M., Zhang, X., & Yan, H. (2011). Unusual salinity conditions in the Yangtze estuary in 2006: Impacts of an extreme drought or of the three Gorges Dam? *Ambio*, *40*(5), 496–505. https://doi.org/10.1007/s13280-011-0148-2

Dangendorf, S., Calafat, F. M., Arns, A., Wahl, T., Haigh, I. D., & Jensen, J. (2014). Mean sea level variability in the north sea: Processes and implications. *Journal of Geophysical Research: Oceans*, *119*(10). https://doi.org/10.1002/2014JC009901

de Nijs, M. A., Winterwerp, J. C., & Pietrzak, J. D. (2008). Chapter 25 spm variations in a harbour basin. In T. Kusuda, H. Yamanishi, J. Spearman, & J. Z. Gailani (Eds.), *Sediment and ecohydraulics* (Vol. 9, pp. 357–378). Elsevier. https://doi.org/10.1016/S1568-2692(08)80027-7

de Nijs, M. A. J., Pietrzak, J. D., & Winterwerp, J. C. (2011). Advection of the salt wedge and evolution of the internal flow structure in the rotterdam waterway. *Journal of Physical Oceanography*, *41*, 3–27. https://doi.org/10.1175/2010jpo4228.1

de Wilde, H. (2024). *Tidal phase differences in multi-branch systems and their effect on salt intrusion* (Vol. 3). Delft University of Technology.

Eslami, S., Hoekstra, P., Kernkamp, H. W. J., Nguyen Trung, N., Do Duc, D., Nguyen Nghia, H., et al. (2021a). Dynamics of salt intrusion in the Mekong delta: Results of field observations and integrated coastal–inland modelling. *Earth Surface Dynamics*, *9*(4), 953–976. https://doi.org/10.5194/esurf-9-953-2021

Eslami, S., Hoekstra, P., Minderhoud, P. S. J., Trung, N. N., Hoch, J. M., Sutanudjaja, E. H., et al. (2021b). Projections of salt intrusion in a mega-delta under climatic and anthropogenic stressors. *Communications Earth & Environment*, *2*(1), 142. https://doi.org/10.1038/s43247-021-00208-5

Eslami, S., Hoekstra, P., Nguyen Trung, N., Ahmed Kantoush, S., Van Binh, D., Duc Dung, D., et al. (2019). Tidal amplification and salt intrusion in the Mekong Delta driven by anthropogenic sediment starvation. *Scientific Reports*, *9*(1), 18746. https://doi.org/10.1038/s41598-019-55018-9

Garcia, A. M. P., Geyer, W. R., & Randall, N. (2022). Exchange flows in tributary creeks enhance dispersion by tidal trapping. *Estuaries and Coasts*, *45*(2), 363–381. https://doi.org/10.1007/s12237-021-00969-4

Gerritsma, A., Verlaan, M., Geraeds, M., Huismans, Y., & Pietrzak, J. (2024). The effects of a storm surge event on salt intrusion: Insights from the Rhine-Meuse Delta. https://doi.org/10.22541/essoar.172227433.30014198/v1

Geyer, W. R. (1997). Influence of wind on dynamics and flushing of shallow estuaries. *Estuarine, Coastal and Shelf Science*, *44*(6), 713–722. https://doi.org/10.1006/ecss.1996.0140

Geyer, W. R., & Ralston, D. K. (2012). *The dynamics of strongly stratified estuaries* (Vol. 2, pp. 37–51). Elsevier Inc. https://doi.org/10.1016/B978-0-12-374711-2.00206-0

Geyer, W. R., Ralston, D. K., & Chen, J.-L. (2020). Mechanisms of exchange flow in an estuary with a narrow, deep channel and wide, shallow shoals. *Journal of Geophysical Research: Oceans*, *125*(12), e2020JC016092. https://doi.org/10.1029/2020JC016092

Geyer, W. R., Trowbridge, J. H., & Bowen, M. M. (2000). The dynamics of a partially mixed estuary. *Journal of Physical Oceanography*, *30*(8), 2035–2048. https://doi.org/10.1175/1520-0485(2000)030⟨2035:TDOAPM⟩2.0.CO;2

Giddings, S. N., Fong, D. A., & Monismith, S. G. (2011). Role of straining and advection in the intratidal evolution of stratification, vertical mixing, and longitudinal dispersion of a shallow, macrotidal, salt wedge estuary. *Journal of Geophysical Research*, *116*(C3), C03003. https://doi.org/10.1029/2010JC006482

Godin, G. (1972). *The analysis of tides*. : University of Toronto Press [Toronto]. (Section: xxi, 264 pages illustrations 26 cm).

Hammond, J. C., Simeone, C., Hecht, J. S., Hodgkins, G. A., Lombard, M., McCabe, G., et al. (2022). Going beyond low flows: Streamflow drought deficit and duration illuminate distinct spatiotemporal drought patterns and trends in the U.S. During the last century. *Water Resources Research*, *58*(9), e2022WR031930. https://doi.org/10.1029/2022WR031930

Hansen, D. V., & Rattray, M. (1965). Gravitational circulation in straits and estuaries.

Hill, A. E., & Souza, A. J. (2006). Tidal dynamics in channels: 2. Complex channel networks. *Journal of Geophysical Research*, *111*(C11), 2006JC003670. https://doi.org/10.1029/2006JC003670

Hong, B., Liu, Z., Shen, J., Wu, H., Gong, W., Xu, H., & Wang, D. (2020). Potential physical impacts of sea-level rise on the pearl river estuary, China. *Journal of Marine Systems*, *201*, 103245. https://doi.org/10.1016/j.jmarsys.2019.103245

Huismans, Y., Leummens, L., Rodrigo, S., Laan, S., Wouter, K., & van der Wijk, R. (2024). *Extra debiet over stuw Hagestein voor het tegengaan van verzilting van de Lek* (Technical Report No. 11210363-001-ZKS-0001). Delft: Deltares.

Jay, D. A. (2010). Estuarine variability. In A. Valle-Levinson (Ed.), *Contemporary issues in estuarine physics* (pp. 62–99). Cambridge University Press.

Jay, D. A., & Dungan Smith, J. (1990). Circulation, density distribution and neap-spring transitions in the Columbia River Estuary. *Progress in Oceanography*, *25*(1–4), 81–112. https://doi.org/10.1016/0079-6611(90)90004-L

Kay, A. L., Bell, V. A., Guillod, B. P., Jones, R. G., & Rudd, A. C. (2018). National-scale analysis of low flow frequency: Historical trends and potential future changes. *Climatic Change*, *147*(3–4), 585–599. https://doi.org/10.1007/s10584-018-2145-y

Korotenko, K. A., Osadchiev, A. A., Zavialov, P. O., Kao, R.-C., & Ding, C.-F. (2014). Effects of bottom topography on dynamics of river discharges in tidal regions: Case study of twin plumes in Taiwan strait. *Ocean Science*, *10*(5), 863–879. https://doi.org/10.5194/os-10-863-2014

Kranenburg, W., van der Kaaij, T., Tiessen, M., Friocourt, Y., & Blaas, M. (2022). Salt intrusion in the rhine Meuse delta: Estuarine circulation, tidal dispersion or surge effect. In *Proceedings of the 39th iahr world congress* (pp. 5601–5608). International Association for Hydro-Environment Engineering and Research (IAHR). https://doi.org/10.3850/IAHR-39WC2521711920221058

Kuijper, K. (2016). *Analyse van de zoutmetingen in november 2015 langs de Hollandsche IJssel—Afleiding dispersiecoefficient* (Technical Report No. 1230077–001). Deltares.

Lee, J., Biemond, B., de Swart, H., & Dijkstra, H. A. (2024). Increasing risks of extreme salt intrusion events across European estuaries in a warming climate. *Communications Earth & Environment*, *5*(1), 60. https://doi.org/10.1038/s43247-024-01225-w

Lee, Y., & Lwiza, K. M. (2008). Factors driving bottom salinity variability in the Chesapeake Bay. *Continental Shelf Research*, *28*(10–11), 1352–1362. https://doi.org/10.1016/j.csr.2008.03.016

Lerczak, J. A., Geyer, W. R., & Chant, R. J. (2006). Mechanisms driving the time-dependent salt flux in a partially stratified estuary. *Journal of Physical Oceanography*, *36*(12), 2296–2311. https://doi.org/10.1175/JPO2959.1

Lerczak, J. A., Geyer, W. R., & Ralston, D. K. (2009). The temporal response of the length of a partially stratified estuary to changes in river flow and tidal amplitude. *Journal of Physical Oceanography*, *39*(4), 915–933. https://doi.org/10.1175/2008JPO3933

Lewis, R., & Lewis, J. (1983). The principal factors contributing to the flux of salt in a narrow, partially stratified estuary. Estuarine. *Coastal and Shelf Science*, *16*(6), 599–626. https://doi.org/10.1016/0272-7714(83)90074-4

Li, Y., & Li, M. (2011). Effects of winds on stratification and circulation in a partially mixed estuary. *Journal of Geophysical Research*, *116*(C12), C12012. https://doi.org/10.1029/2010JC006893

Liu, B., Peng, S., Liao, Y., & Wang, H. (2019). The characteristics and causes of increasingly severe saltwater intrusion in pearl river estuary. *Estuarine, Coastal and Shelf Science*, *220*, 54–63. https://doi.org/10.1016/j.ecss.2019.02.041

MacCready, P. (1999). Estuarine adjustment to changes in river flow and tidal mixing. *Journal of Physical Oceanography*, *29*(4), 708–726. https://doi.org/10.1175/1520-0485(1999)029⟨0708:EATCIR⟩2.0.CO;2

MacCready, P. (2004). Toward a unified theory of tidally-averaged estuarine salinity structure. *Estuaries*, *27*(4), 561–570. https://doi.org/10.1007/BF02907644

MacCready, P. (2007). Estuarine adjustment. *Journal of Physical Oceanography*, *37*(8), 2133–2145. https://doi.org/10.1175/JPO3082.1

MacCready, P., & Geyer, W. R. (2010). Advances in estuarine physics. *Annual Review of Marine Science*, *2*(1), 35–58. https://doi.org/10.1146/annurev-marine-120308-081015

MacVean, L. J., & Stacey, M. T. (2011). Estuarine dispersion from tidal trapping: A New analytical framework. *Estuaries and Coasts*, *34*(1), 45–59. https://doi.org/10.1007/s12237-010-9298-x

Manca, F., Capelli, G., Vigna, F. L., Mazza, R., & Pascarella, A. (2014). Wind-induced salt-wedge intrusion in the tiber river mouth (rome-central Italy). *Environmental Earth Sciences*, *72*, 1083–1095. https://doi.org/10.1007/s12665-013-3024-5

McKeon, M. A., Horner-Devine, A. R., & Giddings, S. N. (2021). Seasonal changes in structure and dynamics in an urbanized salt wedge estuary. *Estuaries and Coasts*, *44*(3), 589–607. https://doi.org/10.1007/s12237-020-00788-z/Published

Monismith, S. G., Kimmerer, W., Burau, J. R., & Stacey, M. T. (2002). Structure and flow-induced variability of the subtidal salinity field in northern san francisco bay. *Journal of Physical Oceanography*, *32*(11), 3003–3019. https://doi.org/10.1175/1520-0485(2002)032⟨3003:SAFIVO⟩2.0.CO;2

Perales-Valdivia, H., Sanay-González, R., & Valle-Levinson, A. (2018). Effects of tides, wind and river discharge on the salt intrusion in a microtidal tropical estuary. *Regional Studies in Marine Science*, *24*, 400–410. https://doi.org/10.1016/j.rsma.2018.10.001

Poggioli, A. R., & Horner-Devine, A. R. (2015). The sensitivity of salt wedge estuaries to channel geometry. *Journal of Physical Oceanography*, *45*(12), 3169–3183. https://doi.org/10.1175/JPO-D-14-0218.1

Ralston, D. K., Geyer, W. R., & Lerczak, J. A. (2008). Subtidal salinity and velocity in the Hudson River Estuary: Observations and modeling. *Journal of Physical Oceanography*, *38*(4), 753–770. https://doi.org/10.1175/2007JPO3808

Ralston, D. K., Geyer, W. R., & Lerczak, J. A. (2010). Structure, variability, and salt flux in a strongly forced salt wedge estuary. *Journal of Geophysical Research*, *115*(C6). https://doi.org/10.1029/2009JC005806

Rijkswaterstaat. (2024a). Hollandsche IJssel. Retrieved from https://www.rijkswaterstaat.nl/water/vaarwegenoverzicht/hollandsche-ijssel

Rijkswaterstaat. (2024b). Lek.

Salcedo-Castro, J., Olita, A., Saavedra, F., Saldías, G. S., Cruz-Gómez, R. C., & De la Torre Martínez, C. D. (2023). Modeling the interannual variability in Maipo and Rapel river plumes off central Chile. *Ocean Science*, *19*(6), 1687–1703. https://doi.org/10.5194/os-19-1687-2023

Schijf, B., & Schönfeld, C. (1953). Theoretical considerations on the motion of salt and freshwater.

Schloen, J., Stanev, E. V., & Grashorn, S. (2017). Wave-current interactions in the southern North Sea: The impact on salinity. *Ocean Modelling*, *111*, 19–37. https://doi.org/10.1016/j.ocemod.2017.01.003

Scully, M. E., Friedrichs, C., & Brubaker, J. (2005). Control of estuarine stratification and mixing by wind-induced straining of the estuarine density field. *Estuarine Research Federation Estuaries*, *28*(3), 321–326. https://doi.org/10.1007/bf02693915

Sherin, V., Durand, F., Papa, F., Islam, A. S., Gopalakrishna, V., Khaki, M., & Suneel, V. (2020). Recent salinity intrusion in the bengal delta: Observations and possible causes. *Continental Shelf Research*, *202*, 104142. https://doi.org/10.1016/j.csr.2020.104142

Stacey, M. T., Burau, J. R., & Monismith, S. G. (2001). Creation of residual flows in a partially stratified estuary. *Journal of Geophysical Research*, *106*(C8), 17013–17037. https://doi.org/10.1029/2000JC000576

van der Weijden, C., & Middelburg, J. (1989). Hydrogeochemistry of the river rhine: Long term and seasonal variability, elemental budgets, base levels and pollution. *Water Research*, *23*(10), 1247–1266. https://doi.org/10.1016/0043-1354(89)90187-5

Warner, J., Schoellhamer, D., Burau, J., & Schladow, G. (2002). Effects of tidal current phase at the junction of two straits. *Continental Shelf Research*, *22*(11), 1629–1642. https://doi.org/10.1016/S0278-4343(02)00026-2

Wilson, B. W. (1960). Note on surface wind stress over water at low and high wind speeds. *Journal of Geophysical Research*, *65*(10), 3377–3382. https://doi.org/10.1029/JZ065i010p03377

Wong, K.-C., & Garvine, R. W. (1984). Observations of wind-induced, subtidal variability in the Delaware estuary. *Journal of Geophysical Research*, *89*(C6), 10589–10597. https://doi.org/10.1029/JC089iC06p10589

Wong, K.-C., & Valle-Levinson, A. (2002). On the relative importance of the remote and local wind effects on the subtidal exchange at the entrance to the Chesapeake Bay. *Journal of Marine Research*, *60*(3), 477–498. https://doi.org/10.1357/002224002762231188

Wunsch, C., & Stammer, D. (1997). Atmospheric loading and the oceanic "inverted barometer" effect. *Reviews of Geophysics*, *35*(1), 79–107. https://doi.org/10.1029/96RG03037

Zhang, X., Hetland, R. D., Marta-Almeida, M., & DiMarco, S. F. (2012). A numerical investigation of the Mississippi and Atchafalaya freshwater transport, filling and flushing times on the Texas-Louisiana Shelf. *Journal of Geophysical Research*, *117*(C11), 2012JC008108. https://doi.org/10.1029/2012JC008108

Zhu, J., Cheng, X., Li, L., Wu, H., Gu, J., & Lyu, H. (2020). Dynamic mechanism of an extremely severe saltwater intrusion in the Changjiang estuary in February 2014. *Hydrology and Earth System Sciences*, *24*(10), 5043–5056. https://doi.org/10.5194/hess-24-5043-2020